ESCUELA TÉCNICA SUPERIOR DE INGENIEROS
INDUSTRIALES Y DE TELECOMUNICACIÓN

UNIVERSIDAD DE CANTABRIA

Trabajo Fin de Grado

Estudio del efecto de los iones divalentes en el comportamiento de la tecnología EDR

(Study of divalent ions effect on the performance of RED technology)

Para acceder al Titulo de

Graduado/a en Ingeniería Química

Autor: Tamara Sampedro Pelayo

ACKNOWLEDGMENT

I would like to express my heartfelt and special gratitude to my supervisors Dr. Lucía Gómez Coma and Dr. Marcos Fallanza Torices for their help, time and valuable guidance in carrying out this project. I greatly appreciate the knowledge they shared with me during these months and the new software tools that have made me known, very useful to enhance and make easier my work. In addition, it is also worth mentioning the opportunity that Advanced Separation Processes group of Chemical and Biomolecular Engineering Department of the University of Cantabria, led by Inmaculada Ortiz, gave me to carry out my final degree project.

I also want to give thanks to the people that helped me in the laboratory tasks, for their aid as well the great moments spent together.

Finally, I really want to thank my parents and close family for giving me encouragement, directly support and trust in me.

TABLE OF CONTENTS

LIST OF FIGURES

LIST OF TABLES

NOMENCLATURE

A	electrode surface area (1.306 cm^2)
AEM	anion exchange membrane
b	cell width (m)
C	salt concentration ($mol \cdot m^{-3}$)
C^A	total anions molar concentration (mol/L)
CE	counter electrode
CEM	cation exchange membrane
CEPM	counter electrode potential measurement
DC	direct contact method
E_{cell}	cell pair voltage (V)

EIS	impedance electrochemical spectroscopy
E_{stack}	stack potential (V)
F	Faraday's constant (96485 $C \cdot mol^{-1}$)
HC	high concentrated compartment
I	electrical current (A)
IEM	ion exchange membrane
J	ion or osmotic flux ($mol \cdot m^{-2} \cdot s^{-1}$)
j	electrical current density ($A \cdot m^{-2}$)
LC	low concentrated compartment
MC	mercury contact method
P	gross power (W)
Q	volumetric flow rate per cell ($m^3 \cdot s^{-1}$)
R	universal gas constant (8.314 $J \cdot mol^{-1} \cdot K^{-1}$)
R^2	correlation reliability (-)
R_A	areal resistance ($\Omega \cdot cm^2$)
R_{AEM}	anion membrane resistance ($\Omega \cdot cm^2$)
R_{AEM}	anion exchange membrane resistance ($\Omega \cdot cm^2$)
R_B	system resistance (Ω)
R_{BL}	boundary layer resistance ($\Omega \cdot cm^2$)
R_{Ca2+}	calcium cation resistance ($\Omega \cdot cm^2$)
R_{cell}	cell pair resistance ($\Omega \cdot cm^2$)
R_{CEM}	cation membrane resistance ($\Omega \cdot cm^2$)
R_{CEM}	cation exchange membrane resistance ($\Omega \cdot cm^2$)

$R_{CEM,Exp}$	experimental cation exchange membrane resistance ($\Omega \cdot cm^2$)
$R_{CEM,Sim}$	simulated cation exchange membrane resistance ($\Omega \cdot cm^2$)
R^{D+}	divalent cations resistance ($\Omega \cdot cm^2$)
RE	reference electrode
RED	reverse electrodialysis
R_{HC}	high concentrated compartment resistance ($\Omega \cdot cm^2$)
R_{LC}	low concentrated compartment resistance ($\Omega \cdot cm^2$)
R_M	membrane resistance (Ω)
R_{Mg2+}	magnesium cation resistance ($\Omega \cdot cm^2$)
R_{Na+}	sodium cation resistance ($\Omega \cdot cm^2$)
$R_{non-ohmic}$	non-ohmic resistance ($\Omega \cdot cm^2$)
R_{ohmic}	ohmic resistance ($\Omega \cdot cm^2$)
R_{stack}	total internal resistance ($\Omega \cdot cm^2$)
$R_{\Delta C}$	bulk solution concentration change resistance ($\Omega \cdot cm^2$)
SGP	salinity gradient power
T	temperature (K)
V_{H_2O}	water molar volume ($m^3 \cdot mol^{-1}$)
WE	working electrode
z	ion valence (-)
α	permselectivity (-)
γ	activity coefficient (-)
x_w^{D+}	divalent cations mass fraction (-)
x_w^{M+}	monovalent cation mass fraction (-)

1. INTRODUCTION

Renewable energy sources are playing a relevant role in the 21st century with an increasing importance, principally due to environmental problems and the need of reaching a sustainable development fulfilling the growing energy demand [1]. The implementation of clean energies is required for reducing global pollution, carbon dioxide emissions responsible of the global warming phenomena and the use of fossil fuels (e.g. oil, coal, natural gas) [2]. Renewable energy is the fastest-growing source of electric power with an annual 2.8% increase [3]. Available sources of renewable energy production that can be harness are: solar, wind, geothermal, biomass, hydro, tidal, wave, and marine currents energy [4].

Salinity Gradient Power (SGP), also termed "Blue Energy", generates electrical or mechanical energy by mixing water streams of different salt concentrations [5]. The spontaneous and irreversible mixing of fresh water and seawater results in an increase in entropy of the system, for harvesting power from the released Gibbs free energy, "controlled mixing" technologies are required [2,4]. Pressure retarded osmosis and Reverse Electrodialysis (RED) are the leading technologies in power generation by means of a salinity gradient [6,7]. Current techniques such as capacitive mixing or nano-fluidic diffusion process are still far from the practical application [2,6].

Reverse Electrodialysis is revealed as the most promising membrane based technology to exploit SGP [5]. RED stack configuration includes cation and anion exchange membranes, CEMs and AEMs respectively, which are positioned alternatively and separated by spacers, as is schematized in **Fig. 1**. The diffusive flux of ions among the Low Concentrated (LC) and High Concentrated (HC) chambers generates an electrochemical membrane potential (ionic current) recorded as a voltage across electrodes, transforming thus the concentration gradient into electrical energy [8,9].

Ion-exchange membranes (IEMs) are key components, the overall cost and efficiency of reverse electrodialysis is directly related to membrane performance. CEMs are negatively charged allowing positive ions to pass through and in AEMs the fixed groups are positively charged so negative ion flux is permitted. Attending to IEMs properties, permselectivity and membrane resistance are the foremost features that characterizes

membrane performance. Other characteristics such as ion exchange capacity, swelling degree or fixed charge density determine the selectively permeate of ions and electrical resistance [10,11]. **Fig. 1** depicts a simplified scheme of the most important components of a RED module.

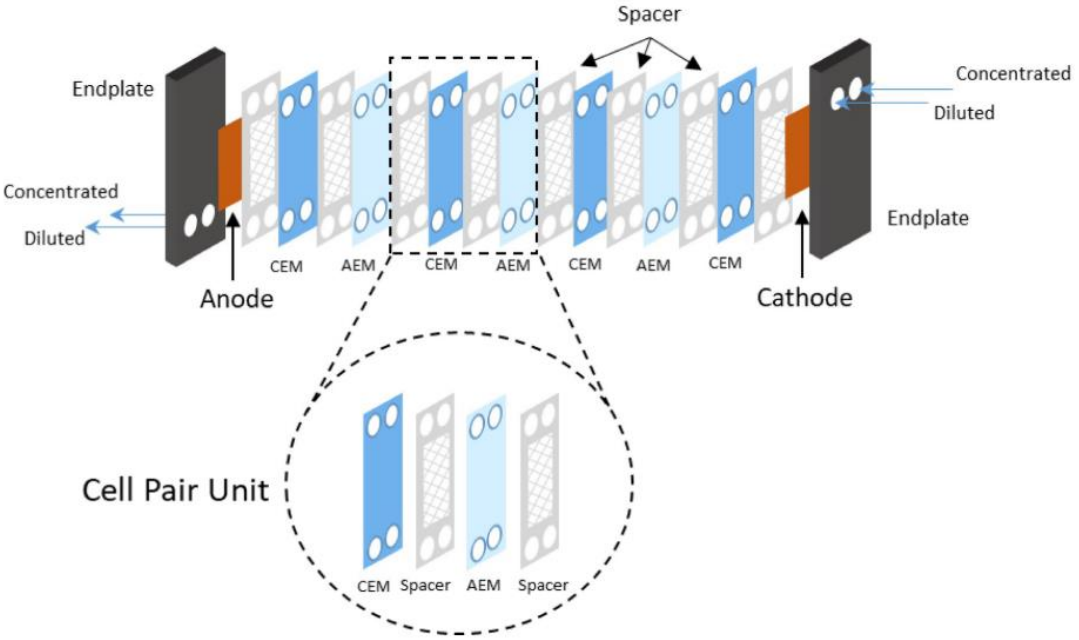

Fig. 1. RED stack schematic diagram [12].

IEM resistance, expressed as areal resistance ($\Omega \cdot cm^2$), is the measure of the degree to which a membrane resists the passage of ionic current through it. Membrane resistance is a restriction for RED systems by modifying power output and consequently the efficiency [13]. Internal resistance of IEMs is affected by solution concentration and composition, temperature and material properties.

Additionally, water stream composition and salinity depends on the origin: natural in case of seawater and river water, anthropogenic for desalination brine or effluent from a wastewater treatment plant and engineered salinity solutions prepared for specific applications [6]. Furthermore, in natural water streams (e.g. river and seawater) divalent ions such as Ca^{2+}, Mg^{2+} and SO_4^{2-} are present, which leads to membrane resistance rising [14].

Considering these factors, there is a necessity of predicting membrane resistance in order to be able of determining the SGP-RED technology performance under different operational conditions and scenarios.

In this context, different experimental measurements to determine empirical correlations that reflects salt concentrations impact on ion exchange membrane resistance are proposed.

1.1. Membrane resistance measurement techniques

A two, three or four electrode system, placed in different configurations, can be used to study the effect of the solution composition on IEMs resistance. The electrochemical-cell setup determines which part of it is characterized by impedance measurements [15].

1.1.1. Two electrode systems

This type of systems presents some advantages in the face of other methods that employs a higher number of electrodes. A two-electrode system present simplicity in the measurement arrangement and robustness of the obtained results [16]. The measurement setups with two electrodes can be differentiated in: direct contact method and indirect or difference method. In both configurations, there are a counter electrode and a working electrode, that also serves as reference electrodes [11].

Direct contact method

The membrane is clamped between the counter electrode and working electrode, ensuring that the applied pressure permits a perfect contact between membrane and electrode. Previously, an equilibration step for the membranes has been carried out, immersing them in the salt solutions for at least 24 h [11,16]. **Fig. 2** represents the cell configuration in direct contact method. Measurements are realized using Electrochemical Impedance Spectroscopy (EIS), afterwards explained in detail in **METHODOLOGY** section.

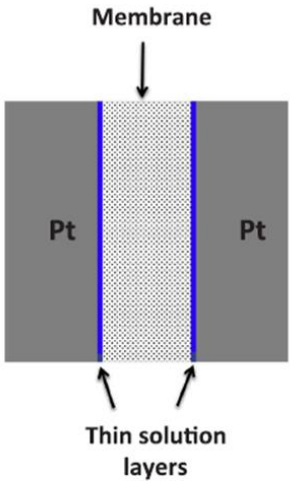

Fig. 2. Cell configuration diagram used in direct contact method. Pt (platinum) refers to the electrode material [11].

Difference method

The salt solution is pumped through the cell compartments located on both membrane sides, which in turn is clamped by plastic pieces. Equilibrating solution for the membranes has the same concentration as the pumped solution. Another requirement for this measurement method is to maintain temperature constant, usually via a circulator bath. Regarding the influence of the solution flow rate, Kamcev et al. proved that modifying this parameter the results are essentially the same, so it could be considered negligible. **Fig. 3**. shows the electrochemical cell configuration used in difference method test by EIS. Membrane resistance is calculated from the difference of the impedance between the cell assembled with membrane and only the salt solution, without membrane [11].

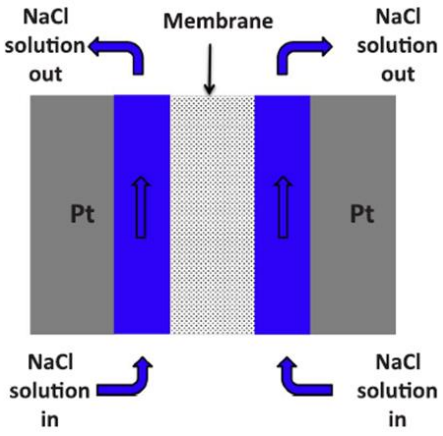

Fig. 3. Cell configuration diagram used in difference method. Pt (platinum) refers to the electrode material [11].

One disadvantage of the two-electrode systems is the influence of low-frequency interfacial polarization phenomena that occurs at the working electrode [15]. In favour of the direct contact method, it should be outlined that on it, is not necessary to quantify solution resistance, the resistance measured corresponds only to the membrane unlike difference technique. For this reason, indirect method complexity is higher.

Mercury Contact Method (MC)

In this technique, the real part of the impedance (R_M), between electrodes submerged in mercury is measured. Mercury operates as an electrode [17], connecting Pt electrodes and membrane sample that has been conditioned previously during 24 h in the salt solution.

High frequencies are required for measuring impedance, since this condition notably reduces mercury/membrane transition interfaces resistance contribution. Among the benefits, MC allows wet and dry samples testing at any temperature as well as membranes with salt deposits on the surface [18].

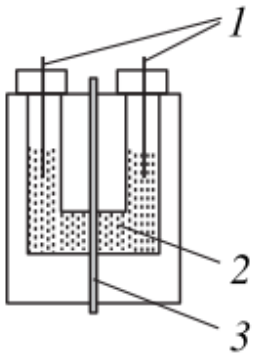

Fig. 4. Cell setup for MC. 1- Pt electrodes, 2-Mercury, 3-Membrane under investigation [18].

Regardless, mercury is an extremely toxic metal and therefore is preferable to employ other techniques for membrane resistance determination in order to avoid human exposure and health hazards.

1.1.1. Three electrode systems

Counter electrode potential measurement (CEPM)

Cyclic Voltammetry is a potential-controlled reversal electrochemical technique. The cell is composed of three electrodes, the working electrode (WE), the counter electrode (CE) and the reference electrode (RE) submerged in an electrolyte solution (**Fig. 5**).

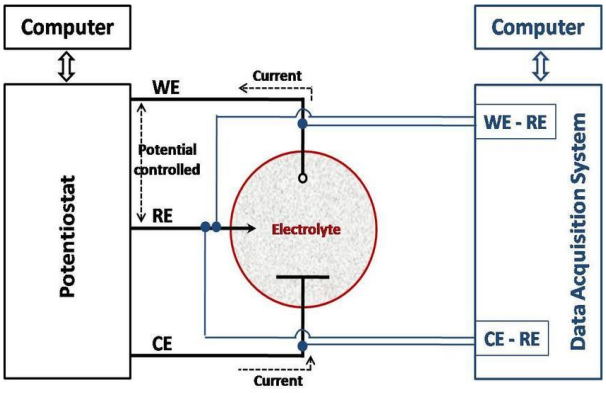

Fig. 5. Diagram for the counter electrode potential measurement by cyclic voltammetry (CE= Counter electrode, WE= Working electrode and RE= Reference electrode) [19].

A cyclic potential is applied to the WE, a reference electrode and the corresponding currents are monitored. The CE serves for measuring potentials related to electrochemical processes, for that a high-impedance voltmeter is used [19]. As result a current vs. potential plot is obtained, with this technique electrochemical cell performance is calculated as an indirect estimation of membrane resistance influence.

1.1.2. Four electrode systems

Four electrode method offers an advantage of reducing interfacial resistance and excluding electrode reactions and polarization, thus, is considered as the most suitable option. However, this procedure can only be carried out with a difference method which is quite difficult to perform at a low external solution salt concentration [11,15,16].

Haber-Luggin capillaries

Galama et al. [16] performed membrane resistance measurements with a four-electrode method in a six-compartment stack. In other studies, it was used an arrangement with two, three or four cell compartments instead of six [10,13,20,21]. The

membrane under investigation is located in the center plane of the stack, hold by insulating plates of PMMA as is shown in **Fig. 6** and separated by four auxiliary membranes from the anode and cathode. Auxiliary membranes function is to prevent solution composition changes produced by reactions taking place on the electrodes at low frequencies.

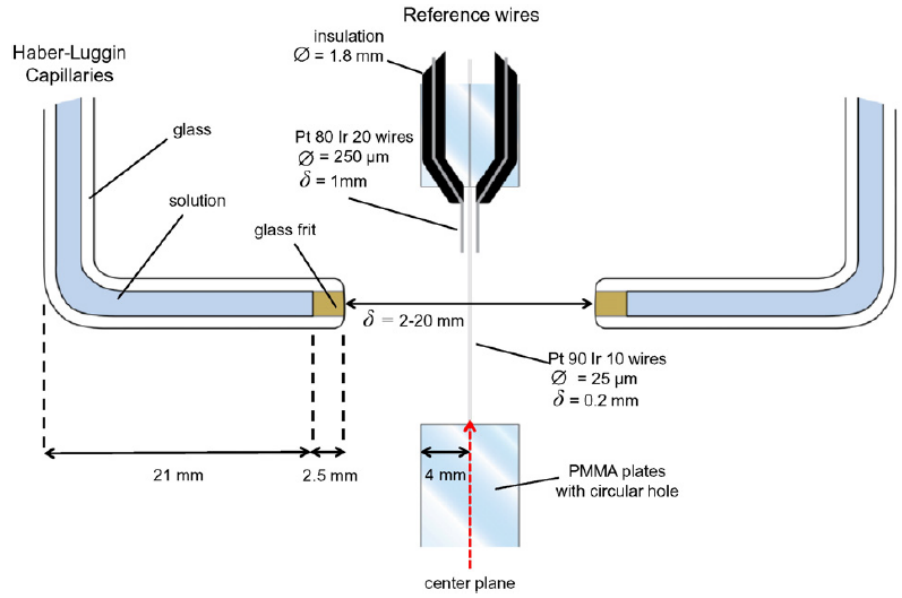

Fig. 6. Scheme of the three sets of reference electrodes: 1) Haber-Luggin capillaries; 2) two platinum iridium (Pt 80/Ir 10) wires; 3) two platinum iridium (Pt 90/Ir 10) wires [16].

Haber-Luggin capillaries serves to situate the sensing point of reference electrodes, that usually are Ag/AgCl electrodes. Concentration polarization is avoided using alternating current at frequencies higher than 0.1 kHz.

As inconvenience these capillaries can suffer gas bubble entrapment and this fact promotes higher impedance due to electrolyte path interruptions. Electrolyte flow from the working electrode to the sensing point of reference electrodes must be assured.

2. THEORY

The model applied in this work was developed by Ortiz-Imedio et al. [12], with the aim of predicting operation variables influence on SGP-RED performance and process costs. This mathematical model comprises mass transfer balances for CEMs and AEMs, water and ions fluxes from concentrated to diluted compartment, cell pair voltage, potential and RED stack resistance.

Mass transfer balances (Eqs. (1–4)) describes salt concentration variation along cell compartments due to ions exchange and water flux.

$$\frac{dC_{HC}^{Na^+}(x)}{dx} = -\frac{b}{Q_{HC_{cell}}(x)} J_{Na^+}(x) + C_{HC}^{Na^+}(x) \frac{bJ_{H_2O}(x)}{Q_{HC_{cell}}(x)} V_{H_2O} \quad (1)$$

$$\frac{dC_{LC}^{Na^+}(x)}{dx} = \frac{b}{Q_{LC_{cell}}(x)} J_{Na^+}(x) - C_{LC}^{Na^+}(x) \frac{bJ_{H_2O}(x)}{Q_{LC_{cell}}(x)} V_{H_2O} \quad (2)$$

$$\frac{dC_{HC}^{Cl^-}(x)}{dx} = -\frac{b}{Q_{HC_{cell}}(x)} J_{Cl^-}(x) + C_{HC}^{Cl^-}(x) \frac{bJ_{H_2O}(x)}{Q_{HC_{cell}}(x)} V_{H_2O} \quad (3)$$

$$\frac{dC_{LC}^{Cl^-}(x)}{dx} = \frac{b}{Q_{LC_{cell}}(x)} J_{Cl^-}(x) - C_{LC}^{Cl^-}(x) \frac{bJ_{H_2O}(x)}{Q_{LC_{cell}}(x)} V_{H_2O} \quad (4)$$

Where **C** is salt concentration (mol·m^{-3}), **b** cell width (m), **Q** volumetric flow rate per cell (m^3·s^{-1}), **J** is ion or osmotic flux (mol·m^{-2}·s^{-1}) and $\mathbf{V_{H_2O}}$ water molar volume (m^3·mol^{-1}).

Stack potential ($\mathbf{E_{stack}}$ in V) is calculated through Eq. (5) and depends on cell pair voltages ($\mathbf{E_{cell}}$), **j** that is electrical current density (A·m^{-2}) and $\mathbf{R_{stack}}$ the total internal resistance (Ω·m^2).

$$E_{stack}(x) = \left(\sum_{i=1}^{N} E_{cell,i}(x)\right) - R_{stack}(x) \cdot j(x) \quad (5)$$

Nernst equation describes cell pair voltage as follows:

$$E_{cell}(x) = \alpha_{CEM} \cdot \frac{R\,T}{F} \cdot \left[\frac{1}{z_i} \ln\left(\frac{\gamma_{HC}^{Na^+}(x) \cdot C_{HC}^{NaCl}(x)}{\gamma_{LC}^{Na^+}(x) \cdot C_{LC}^{NaCl}(x)}\right)\right] + \alpha_{AEM} \cdot \frac{R\,T}{F} \cdot \left[\frac{1}{z_i} \ln\left(\frac{\gamma_{HC}^{Cl^-}(x) \cdot C_{HC}^{NaCl}(x)}{\gamma_{LC}^{Cl^-}(x) \cdot C_{LC}^{NaCl}(x)}\right)\right] \quad (6)$$

Where **α** is membrane permselectivity (-), **R** is the universal gas constant (8.314 J·mol^{-1}·K^{-1}), **T** is the temperature (K), **F** is Faraday's constant (96485 C·mol^{-1}), **z** is the ion valence (-), **γ** is the activity coefficient (-) and **C** is ion concentration (mol·m^{-3}).

The gross power density (**P**, in W) is given by next equation:

$$P(x) = E_{stack}(x) \cdot I(x) \tag{7}$$

where **I** is electrical current (A).

RED stack internal resistance ($\Omega \cdot cm^2$) is the sum of individual cell pairs resistance in series, as express Eq. (8).

$$R_{stack}(x) = \left(\sum_{i=1}^{N} R_{cell,i}(x) \right) \tag{8}$$

For each cell pair resistance Eq. (9) there can be distinguished two parts, an ohmic and a non-ohmic impedance.

$$R_{cell}(x) = R_{ohmic}(x) + R_{non-ohmic}(x) \tag{9}$$

The ohmic part is constituted of the low and high concentrated compartment resistances ($\mathbf{R_{LC}}$ and $\mathbf{R_{HC}}$) and ion exchange membranes resistance ($\mathbf{R_{AEM}}$ and $\mathbf{R_{CEM}}$), in $\Omega \cdot cm^2$. Membrane properties have been considered constant. Regarding non-ohmic term, the resistances associated are $\mathbf{R_{\Delta C}}$ due to the change in bulk solution concentration and boundary layer resistance $\mathbf{R_{BL}}$, attributable to concentration polarization phenomena.

$$R_{ohmic}(x) = R_{HC}(x) + R_{LC}(x) + R_{AEM} + R_{CEM} \tag{10}$$

$$R_{non-ohmic}(x) = R_{\Delta C}(x) + R_{BL}(x) \tag{11}$$

In the developed model, there were established some considerations, among them, the water solutions used only contained sodium chloride. As it was previously mentioned, in natural and anthropogenic water streams there is presence of divalent ions (Mg^{2+}, Ca^{2+} and SO_4^{2-}), therefore, it must be considered their influence in the model parameters.

Multivalent ions decrease cell pair voltage because of valence influence, that affects this variable, and hence have a negative effect on the overall process efficiency. Moreover,

these ions modify anion and cation exchange membrane resistance, which is an undesirable fact in this technology.

The model parameters characterized throughout this study are cation exchange membrane resistance (R_{CEM}) and anion exchange membrane resistance (R_{AEM}).

3. OBJECTIVE

The main purpose of this project is membrane resistance characterisation to enhance previous defined model capability to predict the power output in reverse electrodialysis processes to harvest salinity gradient power, under different operating conditions and scenarios. Thus, it would be possible to determine the efficiency of the process in different locations, since membrane resistance depends on water composition.

In this context, the following objectives are defined in detail:

- to design a measurement system design in order to perform electrochemical experiments using direct contact method.
- to evaluate monovalent and divalent ions influence in membrane resistance.
- to develop correlations able to predict CEM and AEM resistance as a function of monovalent and divalent ions concentration.
- to implement the developed correlations in the model, as well as compare simulated and experimental data obtained in a lab-scale pilot plant.

4. METHODOLOGY

4.1. Materials

Fumasep membranes FKS-50 as CEM and FAS-50 as AEM provided by Fumatech®, were used in this study. The CEMs and AEMs were delivered in H^+ and bromide counter-ion forms, respectively, both membranes with a thickness in the range of 45-55 µm. These commercial membranes accomplish with the requirements for RED applications, having low resistance values and high permselectivity.

4.2. Equipment

4.2.1. Electrochemical workstation

All impedance experiments were performed using the commercial electrochemical workstation Zennium provided by Zahner that includes a potentiostat/galvanostat and a frequency response analyser. **Fig. 7** shows Zennium device and cable connection.

Fig. 7. Electrochemical workstation ZAHNER ZENNIUM.

The system has a total of six connectors for: counter electrode, working electrode, reference electrode, working electrode sense point (S) and two probes. In a two-electrode system the CE and RE are coupled together on one of the electrodes and WE and S on the opposite electrode.

4.3. Solutions

Prior to electrochemical measurements membranes were equilibrated in salt solutions, during at least 24 hours. Solutions have been made with Milli-Q deionized water and the following chemicals reagents: sodium chloride (Merck Millipore, ACS grade) magnesium chloride 6-hydrate (Panreac, pharma grade), calcium chloride (Panreac, pharma grade) and sodium sulfate (Scharlau, ACS grade).

Two series of solutions were prepared. First, solutions containing only one salt for different concentrations in a range between $1 \cdot 10^{-4}$ M and 1 M. The second series is constituted of several NaCl–$MgCl_2 \cdot 6H_2O$ and NaCl–$CaCl_2$ mixtures, for typical salts content in water streams shown in **Table 1**.

Table 1. Usual salts content in different water streams.

	LC solution	Seawater	Brine
NaCl [M]	0.02	0.5	1
Mg^{2+} [M]	0.002	0.06	0.1
Ca^{2+} [M]	0.0015	0.009	0.02
SO_4^{2-} [M]	0.0014	0.03	0.06

4.4. Electrochemical cell design and set-up

A direct contact method was used to realized experimental membrane resistance tests. Due to the necessity of ensuring good contact in the system electrode-membrane-electrode, a new electrochemical cell was designed. Using the software Autodesk AutoCAD® and being based on the stainless-steel electrode available, a piece that fits its size and shape was designed. **Fig. 8**, shows the graphic layout with its dimensions.

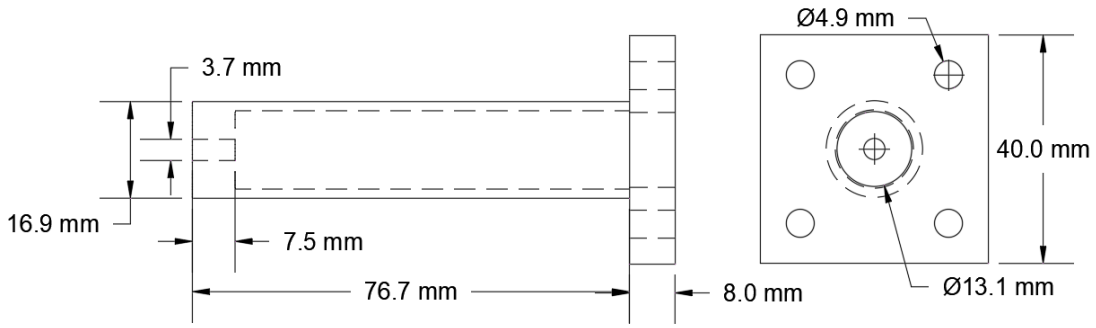

Fig. 8. Piece layout.

The method selected for the manufacture of the pieces was 3D impression and for that purpose the 3D BQ WitBox printer was employed. **Fig. 9** exhibits printing process in PLA (polylactic acid, thermoplastic) material.

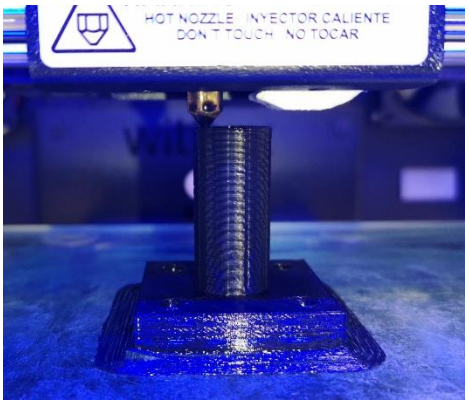

Fig. 9. Intermediate point of 3D printing process.

The general setup schema appears represented in **Fig. 10** and is made up using two equal printed pieces, one of them fixed in a holder and the other which has movement in the vertical axis. Both parts are aligned through four screws (joined to fixed part), working them also as rails for system movement.

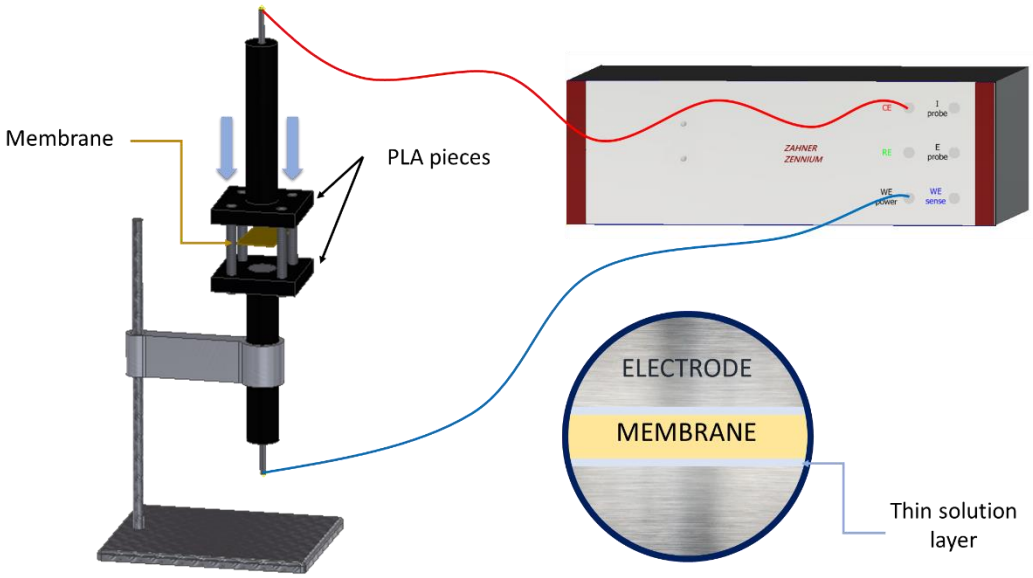

Fig. 10. Experimental arrangement for Electrochemical Impedance Spectroscopy (EIS) membrane resistance measurement.

Concerning system operation mechanism, when the mobile piece is up positioned, the membrane is placed inside, covering the electrode surface. During the measurements, the upper piece is taken down and the membrane is clamped between electrodes only by gravity force.

Finally, wires are connected to working and reference electrodes and EIS experiments can begin. Considering that there is no defined cathode and anode, but the electrodes of the system are defined as working electrode and counter electrode, their connection scheme is not relevant since the potential difference between both is measured.

4.5. Experimental procedure

Once the solutions were prepared, IEMs were cut in a rectangular shape (2 cm length and width) and introduced in the salt solutions. Membranes must be submerged at least 24 hours and at the same measurement temperature, this procedure is named equilibration step. In this case, membranes have been equilibrated at 24℃.

Electrochemical measurements were carried out inside an oven to ensure that results were obtained at 24℃ since temperature affects resistance. The experiment consists in taking the membrane from the solution and quickly clamped between electrodes, when the membrane is well-positioned then EIS measurement can begin. Approximately 40 seconds elapses between removing the membrane from the solution and the measure ends. The time interval is important because if the membrane get dries the final result will be altered. For each solution the experiment was done at least three times, changing membrane sample. After each experiment electrode surface has to be cleaned with deionized water in order to remove the salt remains.

4.6. Electrochemical measurements

Electrochemical Impedance Spectroscopy is an effective technique for IEMs characterization in electrochemical systems. Impedance measurements were performed with the electrochemical workstation Zennium (Zahner) in potentiostatic mode.

EIS experiments were carried out applying an electric current with an amplitude of 10 mV in a frequency range of 100 Hz to 1 MHz. Impedance analyses were controlled and collected by the "Thales" software from Zahner. Data was presented in the form of Bode plot, as shown in **Fig. 11**.

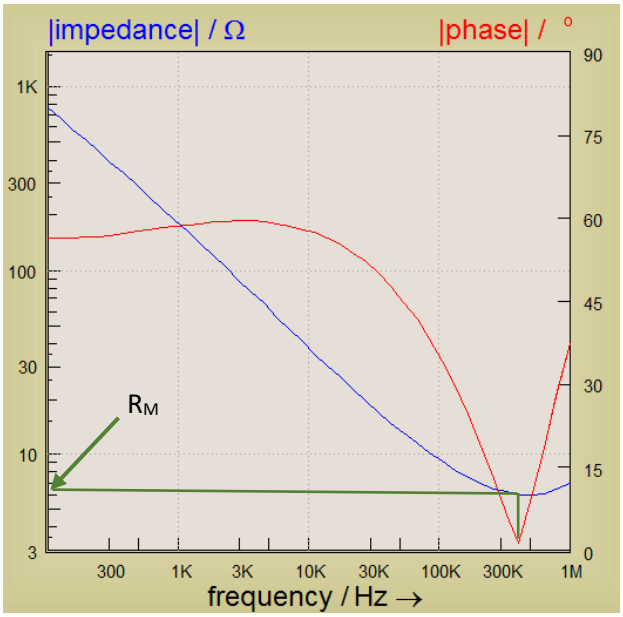

Fig. 11. Bode diagram.

Membrane resistance (**R_M**, in Ω) value corresponds to the real impedance part when the imaginary part (phase) is zero. Results are expressed in terms of membrane areal resistance (**R_A**, in Ω·cm^2), calculated through Eq.(12).

$$R_A = (R_M - R_B) \cdot A \tag{12}$$

where **R_B** is system resistance, blank measurement without membrane (Ω) and **A** is electrode surface area (1.306 cm^2).

5. RESULTS

5.1. Method validation

Before starting with the membrane resistance correlations development, the implemented direct contact method reliability must be proved. In the direct contact method (DC), the presence of thin solution layers between membrane and electrodes or electrode surface faults, getting to worse contact, could have a contribution to the resistance final measured value [11]. These facts are mitigated when using mercury contact method (MC). In order to verify DC experiments, there has been made a comparison between both methods results. Anion exchange membrane resistance values measured with DC and provided data for MC are presented in **Fig. 12** as a function

of external salt concentration (ranging from $1 \cdot 10^{-4}$ to 1M), all experiments were performed at 24℃.

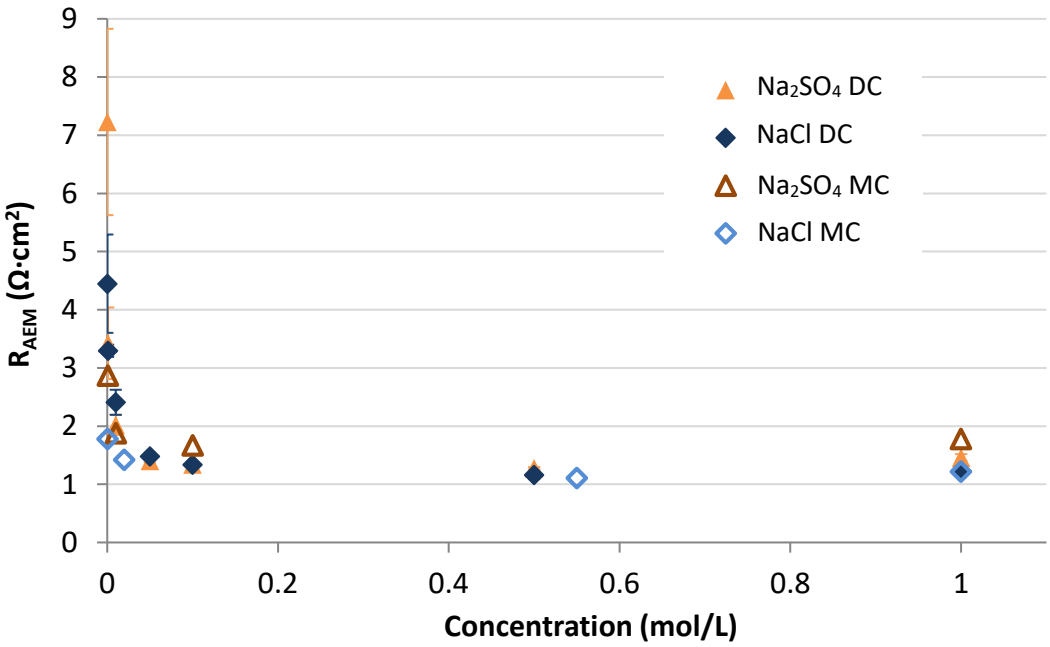

Fig. 12. Anion exchange membrane resistance (R_{AEM}) as function of external salt concentration measured with direct contact method (DC) and provided data using mercury contact method (MC).

For DC method there have been yield good results with a great reproducibility for high salt concentrations in which the error represented in **Fig. 12** is imperceptible. In case of concentrations lower than $1 \cdot 10^{-3}$ M, large measured values variability takes place.

Fig. 13 shows results for cation exchange membrane resistance using DC and data for MC as a function of external salt concentration (ranging from $1 \cdot 10^{-4}$ to 1 M). Concerning CEMs resistance, employing direct contact method the results achieved are reasonably good for almost any salt concentration.

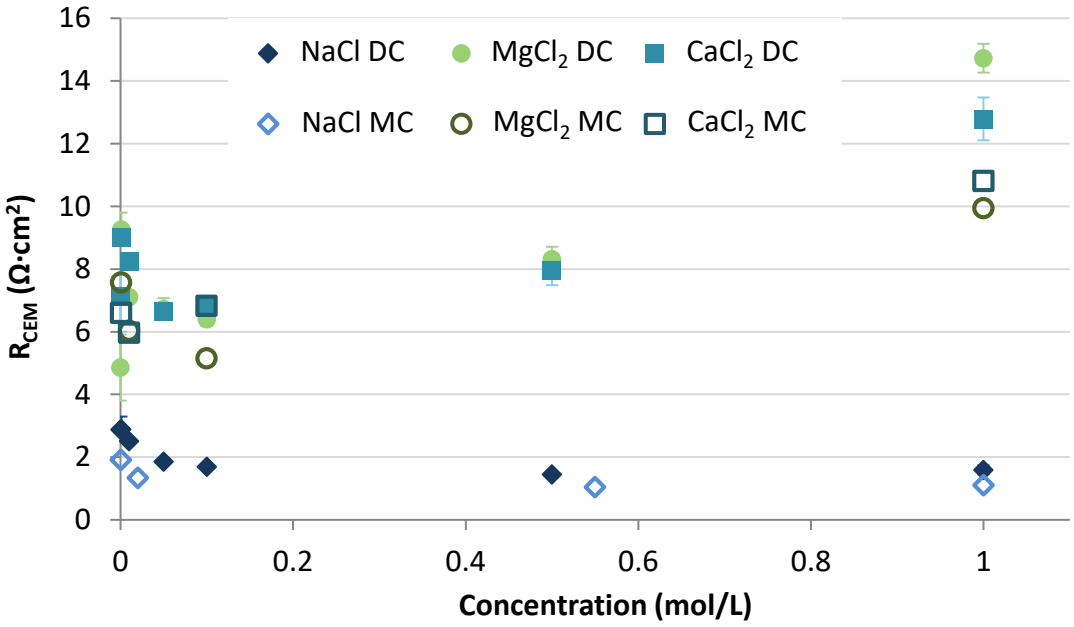

Fig. 13. Cation exchange membrane resistance (R_{CEM}) as function of external salt concentration measured with direct contact method (DC) and provided data using mercury contact method (MC).

Comparing the method proposed in this study and the one employing mercury, no significant deviations are observed between final resistance values. In conclusion, the technique suggested in this study and the experimental system designed provide reliable and robust results and is presented as a great alternative which not employs toxic metals. Additionally, another advantage is measurements simplicity and quickness.

5.2. Analysis of multivalent ions influence

Based on the results presented in **Fig. 12** sulphate anion contribution to membrane resistance rise is trifling or none. By contrast, resistances for the CEM are strongly affected by divalent cations presence. Multivalent ions effects on RED systems are Nernst potential decrease, uphill transport[1] and an increase in electrical membrane resistance.

The increase of membrane resistance in presence of divalent ions can be associated with ions size, for bigger sizes the difficulty to pass through the membrane will increment.

[1] **Uphill transport** in IEMs is known as the process of ion transport against the concentration gradient, meaning from low to high concentrated compartment.

Additionally, another reason of R_M rise is one single divalent cation takes up two membrane fixed charged groups [14].

These results evidence previous defined facts influence and existence as well as highlight more significant influence on CEMs than AEMs.

5.3. R_{AEM} correlation development

Although divalent anions contribution is not an important aspect to consider, anionic membrane resistance needs to be characterised. Since chloride and sulphate ions membrane resistance is the same, according to molar concentration, measured data of **Fig. 12** for Cl^- and SO_4^{2-} taken as a whole were fitted to a correlation in potential form as is shown in Eq. (13).

$$R_{AEM} = 1.107\ (C^A)^{-0.145} \tag{13}$$

where $\mathbf{C^A}$ is total anions molar concentration (mol/L). Extremely low concentration values, unusually present in real water streams, have been excluded. $\mathbf{R^2}$ coefficient gives a measure of correlation reliability. For this correlation the coefficient value is 0.854, which means a reasonable agreement between experimental and predicted data.

5.4. R_{AEM} correlation validation

Given that anionic membrane resistance contribution to ohmic resistance compared with cationic membrane is much lower and divalent anions impact on this parameter is not relevant, R_{AEM} correlation has been proved for three possible scenarios as is gathered in **Table 2**.

Table 2. Experimental and simulated results of R_{AEM} for three different scenarios.

Cl^- [M]	SO_4^{2-} [M]	$R_{AEM,Exp}$	$R_{AEM,Sim}$	Error (%)
0.02	0.001	2.13	1.93	8.9
0.62	0.033	1.38	1.17	14.6
1	0.06	1.63	1.09	32.6

Regarding error values for low and medium salt concentrated solutions tested, the achieved error is lower than 15%, which is in a reasonable range of variation.

Nevertheless, for the highest concentrated scenario the error reaches a value of 32.6%, a fact that may be due to membrane resistance increase observed at concentrations <0.5M. The issue is that R_{AEM} behaviour at high salt concentrations mathematically cannot be described. Therefore and despite this fact, the anionic membrane resistance correlation is validated.

5.5. R_{CEM} correlation development

In this part a correlation describing cation exchange membrane resistance as a function of cation concentration is going to be developed. Eq.(14) expresses the form of this correlation as the resistance's addition of the distinct cations.

$$R_{CEM} = R_{Na^+} + R_{Mg^{2+}} + R_{Ca^{2+}} \tag{14}$$

For that purpose, R_{CEM} (in $\Omega \cdot cm^2$) was evaluated in three different scenarios (1) 0.02 M NaCl (low concentrated stream), (2) 0.5 M NaCl (seawater) and (3) 1 M NaCl (brine). In each scenario, three cases have been studied:

- Typical concentration of divalent cation.

- Half the typical concentration of divalent cation.

- Double the typical concentration of divalent cation.

The influence of magnesium and calcium has been analysed separately. **Fig. 14** presents first scenario results (0.02 M NaCl), R_{CEM} value is increased with Mg^{2+} and Ca^{2+} molar concentration. Apparently, their trends are not related. However, the comparison is in terms of molar concentration, to be comparable, cation size must be taken into consideration.

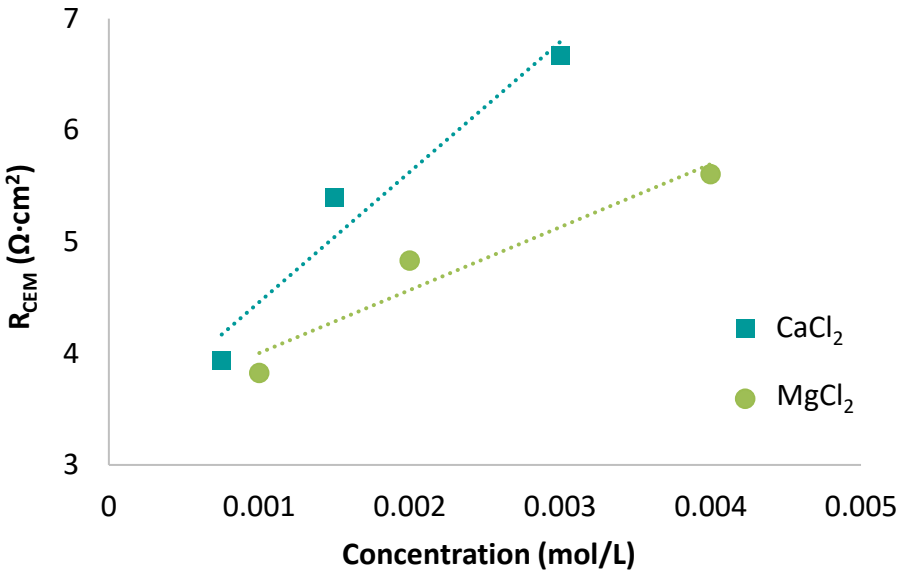

Fig. 14. CEM resistance variation for mixtures of 0.02 M NaCl and different divalent cation concentrations.

In **Fig. 15** the results of **Fig. 14** are presented in mass fraction, that includes cation size by means of the molecular weight (Mg=24.305 g/mol and Ca=40.078 g/mol). The results for 0.5 M NaCl and 1 M NaCl are shown in **Fig. 16** and **Fig. 17**, respectively.

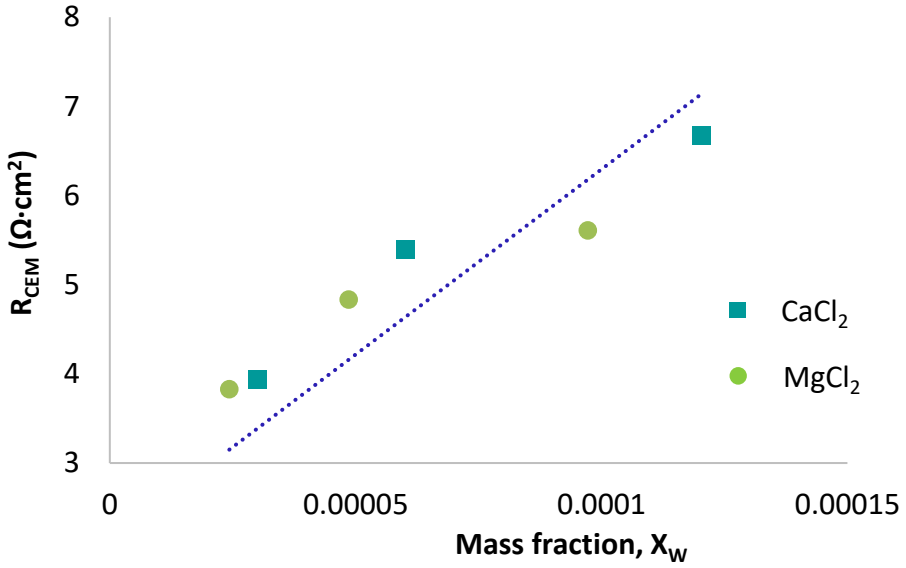

Fig. 15. CEM resistance variation for mixtures of 0.02 M NaCl and different divalent cation mass fractions.

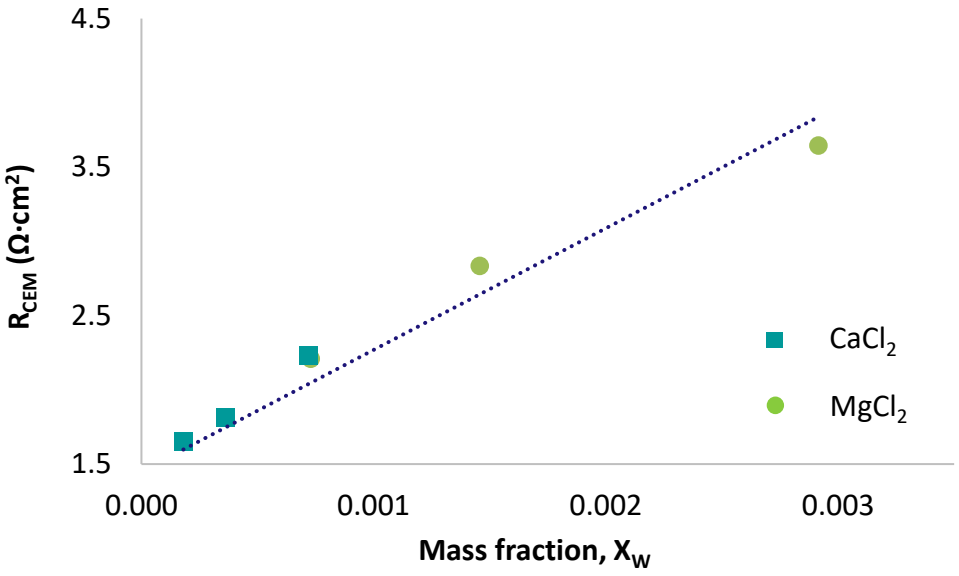

Fig. 16. CEM resistance variation for mixtures of 0.5 M NaCl and different divalent cation mass fractions.

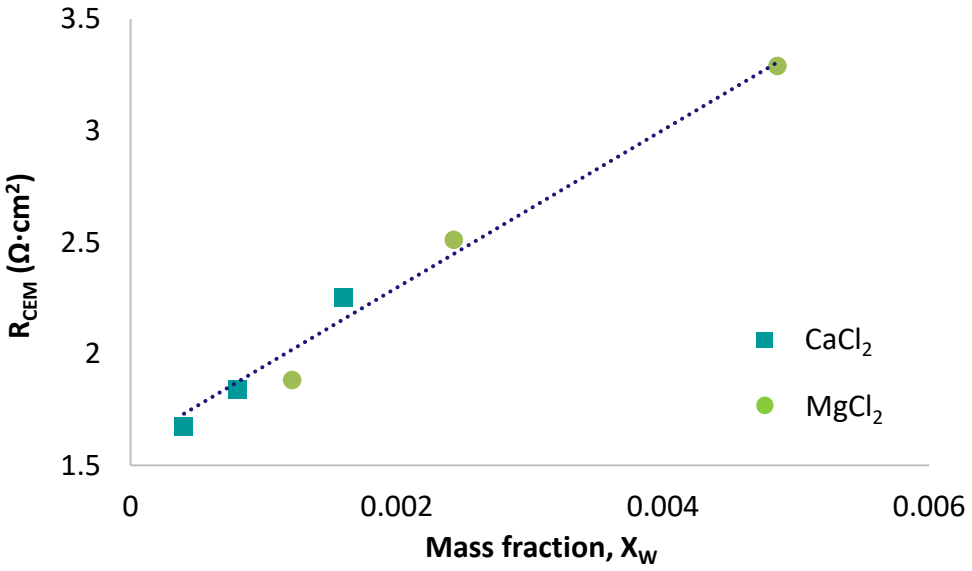

Fig. 17. CEM resistance variation for mixtures of 1 M NaCl and different divalent cation mass fractions.

In all scenarios a highly similar influence of both cations is appreciated. Therefore, from here on it has been assumed their contribution to cationic membrane resistance is the same in terms of mass fraction. For that reason, divalent cation resistance will be considered as the sum of magnesium and calcium resistances. In this way, the Eq. (15) is simplified to the following expression:

$$R_{CEM} = R_{Na^+} + R^{D+} \tag{15}$$

where $\mathbf{R^{D+}}$ is the resistance associated to magnesium and calcium ($\Omega \cdot cm^2$).

Based on previous results, equations have been determined to describe the variation of cation exchange membrane resistance as a function of divalent cations total mass fraction. The resistance behaviour has been considered linear in the range of concentrations studied, even though for much lower concentrations that is not entirely true. These relations, in which sodium cation contribution has been removed, are given by next mathematical linear equations with their respective adjustment values:

$$R^{D+}(0.02\ M\ NaCl) = 41546\ x_w^{D+} \qquad R^2 = 0.603 \tag{16}$$

$$R^{D+}(0.5\ M\ NaCl) = 818.87\ x_w^{D+} \qquad R^2 = 0.945 \tag{17}$$

$$R^{D+}(1\ M\ NaCl) = 353.13\ x_w^{D+} \qquad R^2 = 0.979 \tag{18}$$

where $\boldsymbol{x_w^{D+}}$ is the sum of magnesium and calcium mass fractions (-). Due to low variability in high concentrated solutions tested in scenarios (2) and (3), adjustment coefficients reach values that exhibits a high prediction capacity of their correlations. It should be pointed out that these equations cannot predict R_M for different sodium chloride concentrations only for the fixed values analysed (0.02, 0.5 and 1M).

Furthermore, studied scenarios are compared in order to observe how affects sodium chloride concentration. As is shown in **Fig. 18**, the slope increases contrary to NaCl concentration.

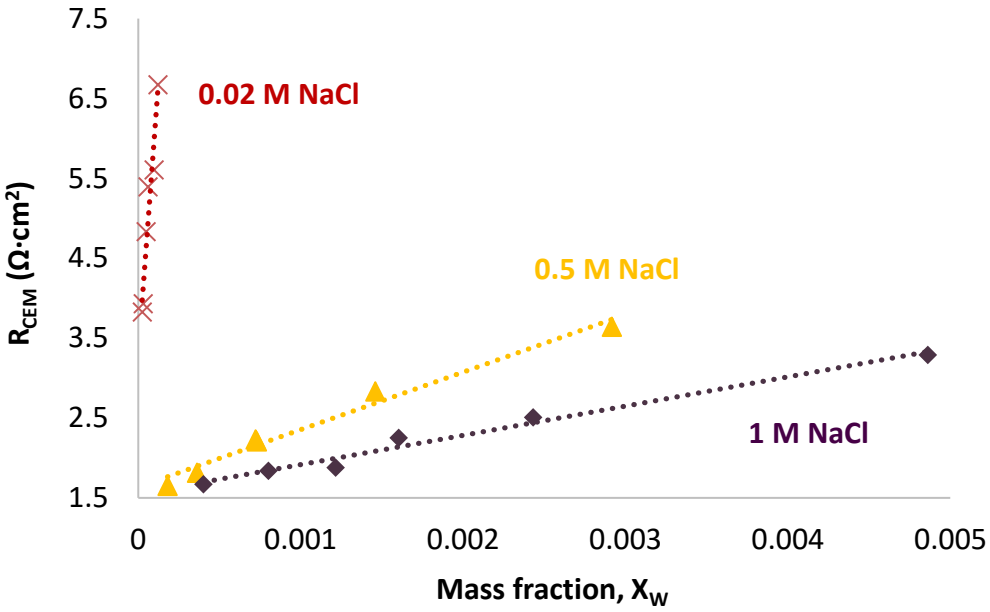

Fig. 18. R_{CEM} dependence of divalent cations mass fraction for different sodium chloride molar concentrations.

With the aim of getting a correlation capable of determining R_{CEM} for any divalent and monovalent cation concentrations, slope according to sodium cation mass fraction has been plotted in **Fig. 19**.

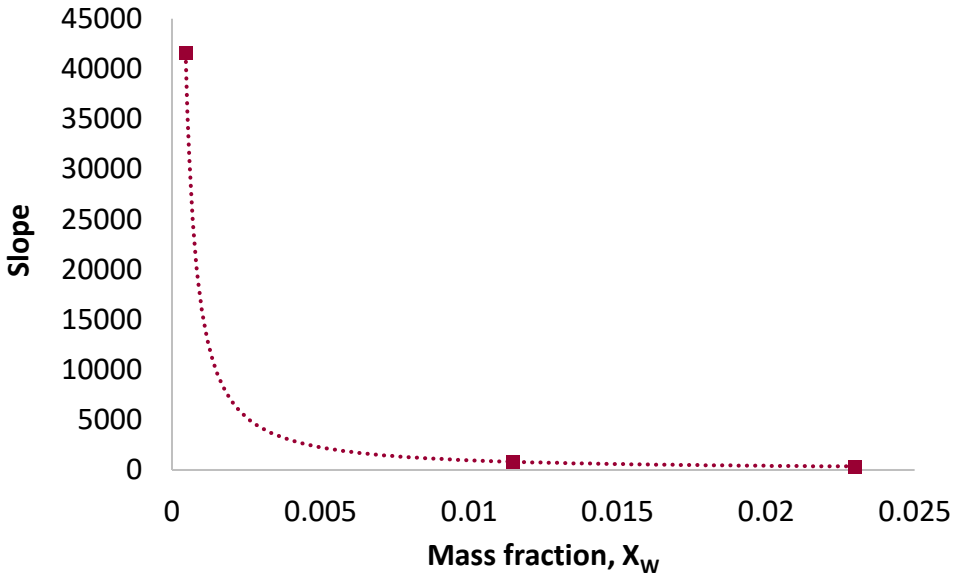

Fig. 19. Slope of divalent cations term in CEM resistance equation as function of sodium chloride mass fraction.

The evolution of slope was fitted to a potential line (R^2=1) mathematically expressed by following equation:

$$Slope = 3.544\ (x_w^{M+})^{-1.219} \tag{19}$$

where $\boldsymbol{x_w^{M+}}$ is monovalent cation mass fraction (-). Subsequently, Eqs. (16-(18) are joined in an only expression substituting slope value by Eq. (19). After this replacement R^{D+} mathematical prediction is given by:

$$R^{D+} = 3.544\ \frac{x_w^{D+}}{(x_w^{M+})^{1.219}} \tag{20}$$

The resistance associated to monovalent cation (Na^+) is defined using the experimental data of **Fig. 13** and characterised by:

$$R_{Na^+} = -0.177 \ln(x_w^{M+}) + 0.785 \qquad R^2 = 0.901 \tag{21}$$

Finally, introducing in Eq. (14) the achieved expressions for divalent and monovalent cations a correlation which predicts cation exchange membrane resistance under different scenarios has been reached and is presented in Eq. (22).

$$R_{CEM} = -0.177 \ln(x_w^{M+}) + 0.785 + 3.544\ \frac{x_w^{D+}}{(x_w^{M+})^{1.219}} \tag{22}$$

5.6. R_{CEM} correlation validation

The validation of the proposed correlation has been carried out through a parity plot. **Fig. 20** shows the comparison between experimental data and predicted values with the correlation developed. The correlation matches with experimental data within an error of ±15 %.

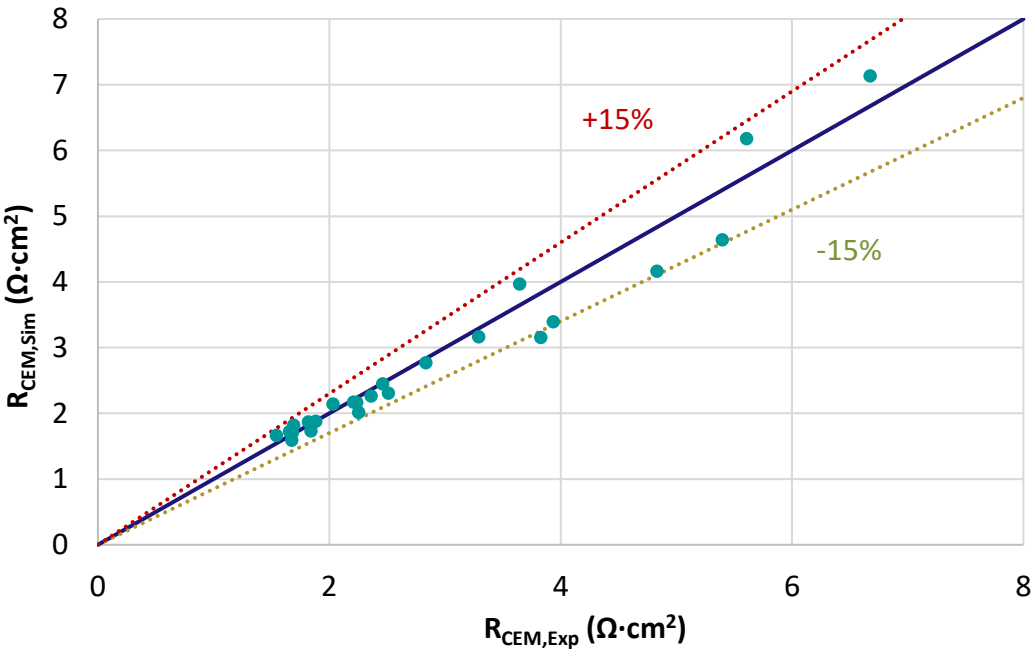

Fig. 20. Parity plot comparing experimental and simulated cation exchange membrane resistance.

Results global error was calculated as the standard deviation with Eq. (23), getting a value of 9.66 %.

$$\sigma = \sqrt{\frac{\sum_{i=1}^{n}\left(\frac{R_{CEM,Exp} - R_{CEM,Sim}}{R_{CEM,Exp}}\right)^2}{n-1}} \qquad (23)$$

where $\mathbf{R_{CEM,Exp}}$ is experimental resistance value and $\mathbf{R_{CEM,Sim}}$ is simulated resistance value (both in Ω·cm^2) and **n** is the number of experiments.

In view of these results, cation exchange membrane resistance correlation is considered valid and capable of predicting membrane resistance for different salt concentrations in water streams.

5.7. Model simulation

Having been implemented the anionic and cationic membrane resistance correlations in the mathematical model and considering divalent ions presence, different scenarios have been considered. These are the scenarios studied:

(1) High concentrated compartment: First brine of a desalination plant (usual NaCl molarity 1)

(2) High concentrated compartment: Seawater (Mediterranean Sea, NaCl 0.5M)

in both for the low concentrated compartment a second brine of a desalination plant (usual NaCl molarity 0.02) was used, this stream corresponds to the retentate when the first permeate passes through a second reverse osmosis stage.

In **Fig. 21** appear represented the results simulated with the model and experimental data of a RED lab-scale pilot plant, comparing the power output for water streams only with monovalent ions (ideal situation) and including divalent ions influence (real situation).

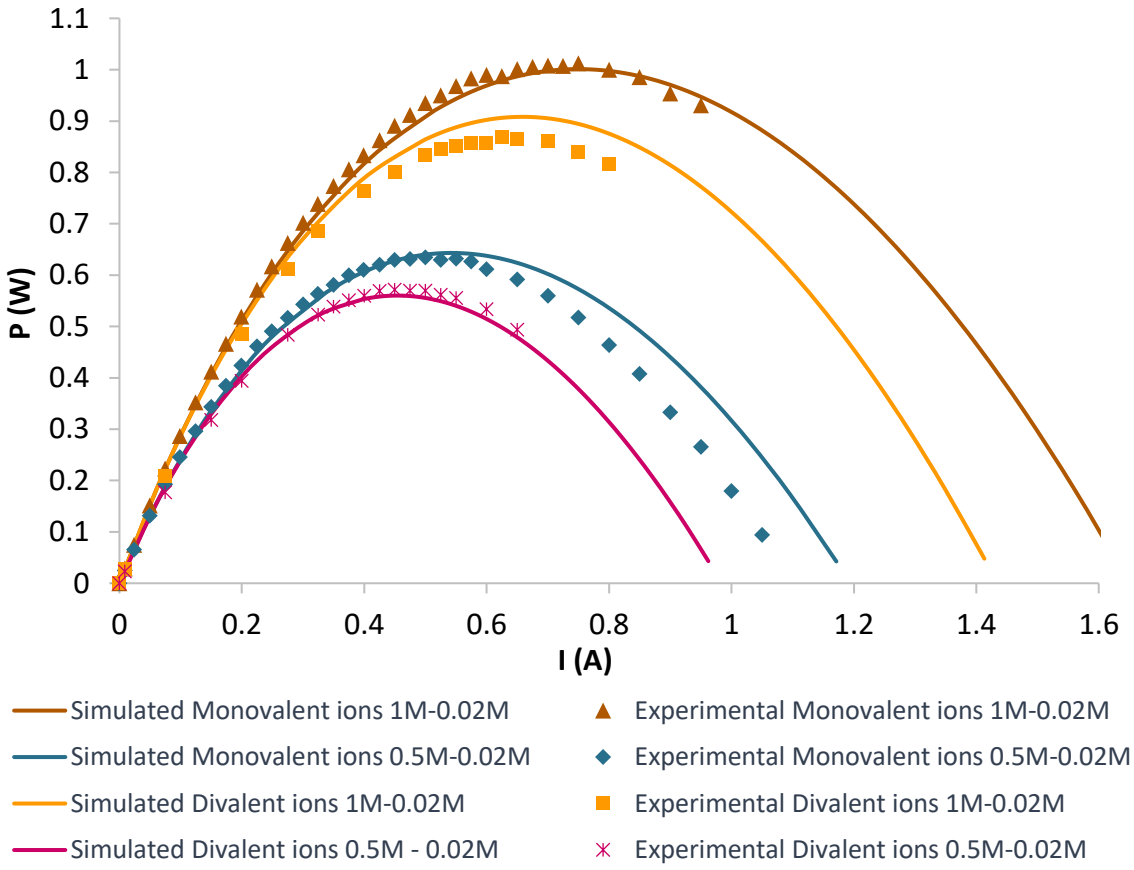

Fig. 21. Gross power vs electrical current for different scenarios.

In the first scenario (1 M-0.02 M), the maximum gross power determined through the model is 0.908W. Comparing simulated value with experimental maximum gross power the error is 4.53%. Making the same comparison for the second scenario (0.5 M-0.02 M) the error between simulated and experimental data is lower 1.99%, reaching a maximum simulated power output of 0.56W. These errors exhibit a really good agreement between simulated and experimental data.

Furthermore, including real salt contents in water streams the gross power has been reduced 9.19% and 12.89% for first and second scenario, respectively, which indicates a remarkable influence of divalent ions in process efficiency.

Regarding salinity gradient, a higher power production is observed in case of employing desalination brines, due to a higher salinity difference.

6. CONCLUSIONS

According to the established objectives, it can be concluded that the measurement system designed provides reliable and robust results with a good reproducibility, employing a direct contact method characterised by simplicity and quickness in the experiments procedure, providing thus a useful and health safe method for membrane resistance measurement.

The influence of divalent ions in ion exchange membrane resistance has been proved, primarily in the cation exchange membrane.

The correlations developed for cationic and anionic membrane resistance prediction are able of determining these parameters for any monovalent and divalent salt concentration, within a reasonable error range.

The mathematical model prediction capability has increased showing a power output reduction in presence of divalent ions, being able to offer maximum gross power results with an error of less than 5% compared to the experimental one.

In conclusion, the mathematical model has been enhanced after including membrane resistance dependence with monovalent and divalent ions and is able to predict reverse electrodialysis performance for salinity gradient power harnessing under different operation conditions and considering different real scenarios.

In further studies, the influence of temperature on ion exchange membrane resistance is suggested to be evaluated, as well as exploring power potential in water streams of diverse origins such as brackish water or the wastewater treatment plant effluent in different combinations with seawater and desalination brines, leading to distinct salinity

gradients and determining the best feasible option to produce clean power through SGP-RED technology.

7. REFERENCES

[1] P. Długołecki, K. Nymeijer, S. Metz, M. Wessling, Current status of ion exchange membranes for power generation from salinity gradients, J. Memb. Sci. 319 (2008) 214–222. doi:10.1016/j.memsci.2008.03.037.

[2] Z. Jia, B. Wang, S. Song, Y. Fan, Blue energy: Current technologies for sustainable power generation from water salinity gradient, Renew. Sustain. Energy Rev. 31 (2014) 91–100. doi:10.1016/j.rser.2013.11.049.

[3] A.H. Avci, R.A. Tufa, E. Fontananova, G. Di Profio, E. Curcio, Reverse Electrodialysis for energy production from natural river water and seawater, Energy. 165 (2018) 512–521. doi:10.1016/j.energy.2018.09.111.

[4] G. Micale, A. Cipollina, A. Tamburini, Salinity gradient energy, Elsevier Ltd., 2016. doi:10.1016/B978-0-08-100312-1.00001-8.

[5] R.A. Tufa, S. Pawlowski, J. Veerman, K. Bouzek, E. Fontananova, G. di Profio, S. Velizarov, J. Goulão Crespo, K. Nijmeijer, E. Curcio, Progress and prospects in reverse electrodialysis for salinity gradient energy conversion and storage, Appl. Energy. 225 (2018) 290–331. doi:10.1016/j.apenergy.2018.04.111.

[6] N.Y. Yip, D. Brogioli, H.V.M. Hamelers, K. Nijmeijer, Salinity gradients for sustainable energy: Primer, progress, and prospects, Environ. Sci. Technol. 50 (2016) 12072–12094. doi:10.1021/acs.est.6b03448.

[7] G. Mehta, S. Jain, M. Fraser, S. Senatore, H. Rothstein, Salinity Gradient Energy Conversion, (2005) 566–571. doi:10.1109/oceans.1979.1151215.

[8] A.H. Avci, P. Sarkar, D. Messana, E. Fontananova, G. Di Profio, E. Curcio, Effect of MgCl2 on Energy Generation by Reverse Electrodialysis, Int. Conf. Nanotechnol. Based Innov. Appl. Environ. 47 (2016) 361–366. doi:10.3303/CET1647061.

[9] T. Rijnaarts, J. Moreno, M. Saakes, W.M. de Vos, K. Nijmeijer, Role of anion exchange membrane fouling in reverse electrodialysis using natural feed waters, Colloids Surfaces A Physicochem. Eng. Asp. 560 (2019) 198–204. doi:10.1016/j.colsurfa.2018.10.020.

[10] Y. Mei, C.Y. Tang, Recent developments and future perspectives of reverse electrodialysis technology: A review, Desalination. 425 (2018) 156–174. doi:10.1016/j.desal.2017.10.021.

[11] J. Kamcev, R. Sujanani, E.S. Jang, N. Yan, N. Moe, D.R. Paul, B.D. Freeman, Salt concentration dependence of ionic conductivity in ion exchange membranes, J. Memb. Sci. 547 (2018) 123–133. doi:10.1016/j.memsci.2017.10.024.

[12] R. Ortiz-Imedio, L. Gomez-Coma, M. Fallanza, A. Ortiz, R. Ibañez, I. Ortiz, Comparative performance of Salinity Gradient Power-Reverse Electrodialysis under different operating conditions, Desalination. 457 (2019) 8–21. doi:10.1016/j.desal.2019.01.005.

[13] S. Zhu, R.S. Kingsbury, D.F. Call, O. Coronell, Impact of solution composition on the resistance of ion exchange membranes, J. Memb. Sci. 554 (2018) 39–47. doi:10.1016/j.memsci.2018.02.050.

[14] T. Rijnaarts, E. Huerta, W. Van Baak, K. Nijmeijer, Effect of Divalent Cations on RED Performance and Cation Exchange Membrane Selection to Enhance Power Densities, Environ. Sci. Technol. 51 (2017) 13028–13035. doi:10.1021/acs.est.7b03858.

[15] V.F. Lvovich, Impedance Spectroscopy, Applications to Elechtrochemical and Dielectric Phenomena, First, Wiley, Hoboken, New Jersey (U.S.A.), 2012.

[16] A.H. Galama, N.A. Hoog, D.R. Yntema, Method for determining ion exchange membrane resistance for electrodialysis systems, Desalination. 380 (2016) 1–11. doi:10.1016/j.desal.2015.11.018.

[17] D.R. Díaz, F.J. Carmona, L. Palacio, N.A. Ochoa, A. Hernández, P. Prádanos, Impedance spectroscopy and membrane potential analysis of microfiltration membranes. The influence of surface fractality, Chem. Eng. Sci. 178 (2018) 27–38. doi:10.1016/j.ces.2017.12.027.

[18] L. V. Karpenko, O.A. Demina, G.A. Dvorkina, S.B. Parshikov, C. Larchet, B. Auclair, N.P. Berezina, Comparative study of methods used for the determination of electroconductivity of ion-exchange membranes, Russ. J. Electrochem. 37 (2001)

287–293. doi:10.1023/A:1009081431563.

[19] D. Vishnu, N. Sanil, K. Mohandas, Measurement of Counter Electrode Potential during Cyclic Voltammetry and Demonstration on Molten Salt Electrochemical Cells, Int. Res. J. Pure Appl. Chem. 15 (2017) 1–13. doi:10.9734/irjpac/2017/37175.

[20] P. Sistat, A. Kozmai, N. Pismenskaya, C. Larchet, G. Pourcelly, V. Nikonenko, Electrochimica Acta Low-frequency impedance of an ion-exchange membrane system, 53 (2008) 6380–6390. doi:10.1016/j.electacta.2008.04.041.

[21] I. Herraiz-Cardona, E. Ortega, V. Pérez-Herranz, Evaluation of the Zn2+ transport properties through a cation-exchange membrane by chronopotentiometry, J. Colloid Interface Sci. 341 (2010) 380–385. doi:10.1016/j.jcis.2009.09.053.